Journal of Cleaner Production 292 (2021) 126034

Contents lists available at ScienceDirect

Journal of Cleaner Production

journal homepage: www.elsevier.com/locate/jclepro

The turning point between urban vegetation and artificial surfaces for their competitive effect on land surface temperature

Yue Liu [a], Xin Huang [a, b, *], Qiquan Yang [a], Yinxia Cao [a]

[a] School of Remote Sensing and Information Engineering, Wuhan University, Wuhan, 430079, PR China
[b] State Key Laboratory of Information Engineering in Surveying, Mapping and Remote Sensing, Wuhan University, Wuhan, 430079, PR China

ARTICLE INFO

Article history:
Received 23 June 2020
Received in revised form
5 January 2021
Accepted 16 January 2021
Available online 20 January 2021

Handling editor Bin Chen

Keywords:
Urban thermal environment
Warming effect
Cooling effect
High-resolution
Background climate
Remote sensing

ABSTRACT

As the two most common types of land cover in cities, vegetation (Veg) and artificial surfaces (AS) often exhibit competitive effects, i.e., cooling effect and warming effect, on land surface temperature (LST). Hitherto, the change of this competitive effect along the proportion gradient of AS within urban areas and their implications for urban construction still lacks adequate attention and discussion. To fill this gap, we made a quantitative analysis of the relationship between Veg (trees or grassland), AS and LST in 35 major cities of China by using Ziyuan-3 (ZY-3) high-resolution satellite observations. Results found that: (1) in each city, there exists a certain threshold (or "turning point") along the proportion gradient of AS, exceeds which AS replaces Veg as the variable that have dominant effect on LST (i.e., the warming effect of AS is always stronger than the cooling effect of Veg); (2) for most cities, the turning points of AS for grassland and trees are 60% and 70%, respectively; (3) the turning point for cities at a higher development level is lower, indicating that even a relatively low AS coverage (~50–60%) in these areas can lead to an evident rise in LST; 4) compared to cities in temperate and tropical climate zones, the turning point for arid/semi-arid cities is higher, implying that their urban Veg shows a better performance in mitigating urban heat stress. This study represents a systematic investigation of the competitive effect of urban Veg and AS on LST, and the understanding of turning point provides a new perspective for stakeholders to integrate urban development and temperature regulation in planning initiatives.

1. Introduction

Urban development has had a great effect on urban microclimate changes worldwide, and is often accompanied by the urban heat island (UHI) effect owing to the replacement of vegetation (Veg) with artificial surfaces (AS) (Yang et al., 2018). The rising temperature increases the risk of heat exposure for urban dwellers. Studies have shown that high-temperature events (e.g., heat waves) are closely associated with a range of fatal heat-sensitive diseases (Shahmohamadi et al., 2011) and unsatisfactory socio-economic factors (Santamouris and Kolokotsa, 2015; Carleton and Hsiang, 2016). In this context, understanding the underlying mechanism of how Veg and AS jointly affect the land surface temperature (LST) is in urgent need to alleviate the UHI effect and protect residents who are vulnerable to extreme heat, especially in summer daytime.

The advent of remote sensing (RS) technology enables long-term and large-scale observations of LST and provides explicitly spatial data sets of land cover and land use (LCLU). Based on this, intensive related researches have proved that the spatial heterogeneity of LST distribution is significantly related to the various composition of urban land covers, particularly the Veg and AS (Maimaitiyiming et al., 2014; Zhou et al., 2014; Tran et al., 2017). When Veg and AS co-occur in a region, it is often considered that these two land-cover categories show a competitive effect (i.e., the Veg-induced cooling effect and AS-induced warming effect) on LST, and the result of this so-called competition (i.e., the net effect) determines the change of LST (Ziter et al., 2019). Nevertheless, there are two major issues have not been clearly clarified in the extant literature. On the one hand, the quantitative changes of this competitive effect for different combinations of Veg and AS on LST remain unclear. On the other hand, there lacks a bridge to connect our understanding of the competitive effect with the needs of actual urban planning.

* Corresponding author. School of Remote Sensing and Information Engineering, Wuhan University, Wuhan 430079, PR China.
E-mail addresses: yliu_rs@whu.edu.cn (Y. Liu), xhuang@whu.edu.cn (X. Huang), yqq@whu.edu.cn (Q. Yang), 542799173@qq.com (Y. Cao).

https://doi.org/10.1016/j.jclepro.2021.126034
0959-6526/

Accordingly, in this study, we propose an assumption that a threshold exists with regard to the proportion of Veg or AS in their competitive process, at which point the dominant feature affecting LST changes. To better elaborate it, we layout a conceptual diagram of the proposed assumption (Fig. 1). It has been agreed that with the increment of the proportion of AS, the positive effect of AS on LST is gradually enhanced but, instead, the negative effect of Veg is weakened by degrees (Estoque et al., 2017). When the proportion of AS exceeds a certain threshold, the category that has a dominant effect on LST is AS, and otherwise the Veg dominates LST. This threshold can be viewed as the "turning point" between AS and Veg, which can not only serve as an intuitive and effective indicator to quantitatively reflect their competitive effect on LST, but also provides inspiring implications for stakeholders to balance urban construction and temperature regulation.

Some previous studies have also attempted to discuss the appropriate proportions of Veg or AS to maintain a pleasant urban LST. For instance, through on-site survey and numerical modeling, Moriyama and Tanaka (2009) and Ng et al. (2012) found that the temperature dropped significantly when the tree coverage reached around 30% in Hong Kong, China, and Osaka, Japan, respectively. Ziter et al. (2019) adopted a bicycle-mounted measurement system and observed that the canopy cooled the temperature greatest when its cover exceeded 40% in Madison, U.S. Alavipanah et al. (2015) obtained an optimal Veg fraction of 70–80% in Munich, Germany, for mitigating the LST and Xu et al. (2013) suggested that the impervious surface of Xiamen, China should not exceed 70% of the urban area. However, it should be noted that urban areas are often regarded as a mixture of various landscapes. In the same region, LST is not only affected by a single landscape of Veg or AS, but by their complicated interactions (Trlica et al., 2017). From this perspective turning point is proposed integrating these two land cover categories so as to meet the needs and wants of those who formulate the policies. More importantly, limited by the data availability, current researches focus largely on the analysis of individual cities, which is not conducive to establishing a general pattern of the competitive effects of Veg and AS on LST. Out of the same reason, low- and medium-resolution remote sensing imageries are prevailing data sources for most of these researches. Based on these coarse-resolution classification datasets, the optimal combination of Veg and AS required for cooling the urban LST can be overestimated as some small and scattered landscape patches are ignored.

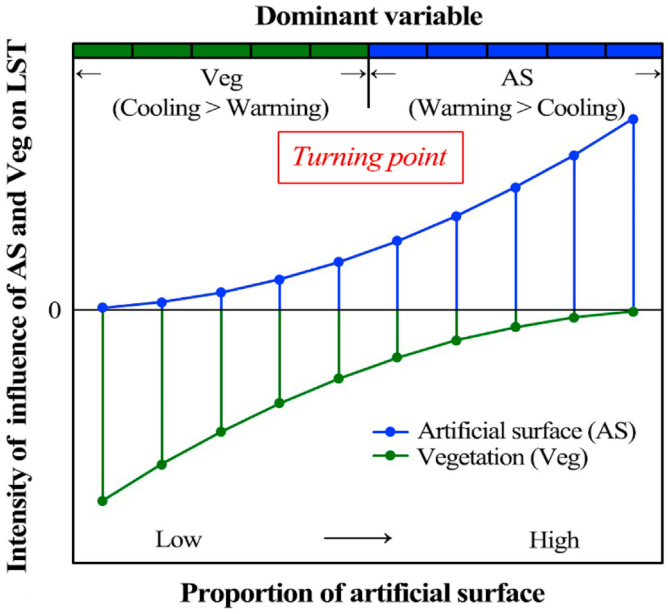

Fig. 1. A conceptual diagram showing the impact of Veg (green) and AS (blue) on LST under different proportions of AS. In this graph, when the proportion of AS is low, the cooling effect of Veg is stronger than the warming effect of AS, and Veg is the dominant variable; when the proportion of AS is higher than the turning point, the situation is reversed.

Therefore, to solve these issues exist in previous studies, this study firstly selected 35 typical cities in China as the study area based on the consideration that the variations in the hydrothermal environment and the development levels between cities may lead to discrepancies in the nature of Veg and AS (Zhou et al., 2017a,b). Secondly, this study produced classification maps of the 35 cities on the basis of Ziyuan-3 (ZY-3) high-resolution remote sensing images (with a 2.1-m resolution) to depict the precise distribution characteristics of urban AS and Veg, which is rare in the existing researches. Another highlight in this study is that we investigated the joint effect of AS and Veg on LST from the perspective of competition and obtained the turning point in a quantitative way.

Overall, we aimed to: 1) assess the joint effects of Veg (trees or grassland) and AS on LST by quantitatively exploring the proportion of Veg or AS that can have a dominant effect on LST; and 2) investigate the 35 major cities of China to reveal the general patterns of such joint effects and their variations in different climate zones and development levels.

2. Study area

China is the third largest country in the world in terms of land area (~9.6 million km^2), extending from 73°33′ E to 135°05′ E and 3°51′ N to 53°33′ N. This vast territory provides space for the growth of Veg, and the various climate types are beneficial for maintaining the diversity of plant species. According to Olson's biome designation (Olson et al., 2001), China spans three climate zones, as shown in Fig. 2(A): 1) the tropical climate zone (mainly evergreen broad-leaved forest and mangroves); 2) the temperate climate zone (mainly deciduous broad-leaved forest and mixed forest); and 3) the arid/semi-arid climate zone (mainly coniferous forest and grassland). Urbanization, as a typical case of human activity induced land-cover change, has been prevalent in the cities of China for decades. The growth or change (to AS) of vegetation is heavily affected by the intensity of urbanization and varies significantly across geographical regions. Considering the complicated and diverse urban landscapes, China is an ideal study area for exploring the relationship between urban vegetation (Veg), artificial surfaces (AS), and LST (hereinafter referred to as the "Veg-AS-LST relationship").

The 35 major cities of China were selected for the study, including 22 provincial capitals, four municipalities, one special economic zone, and eight other major cities. All these cities have witnessed the rapid urbanization process in China and the subsequent changes in the urban landscape and thermal environment. To further investigate the difference of the Veg-AS-LST relationship, we categorized the 35 cities into super first-tier, first-tier, second-tier, and third-tier city, based on the city ranking list (China Business Network Co., Ltd, 2019).

3. Data and methods

3.1. High-resolution land cover mapping

The Ziyuan-3 (ZY-3) satellite, which was launched in January 2012, is China's first high-resolution stereo mapping satellite. Its panchromatic (PAN) and multi-spectral (MS) cameras provide one PAN band (2.1-m spatial resolution) and four MS bands (5.8-m

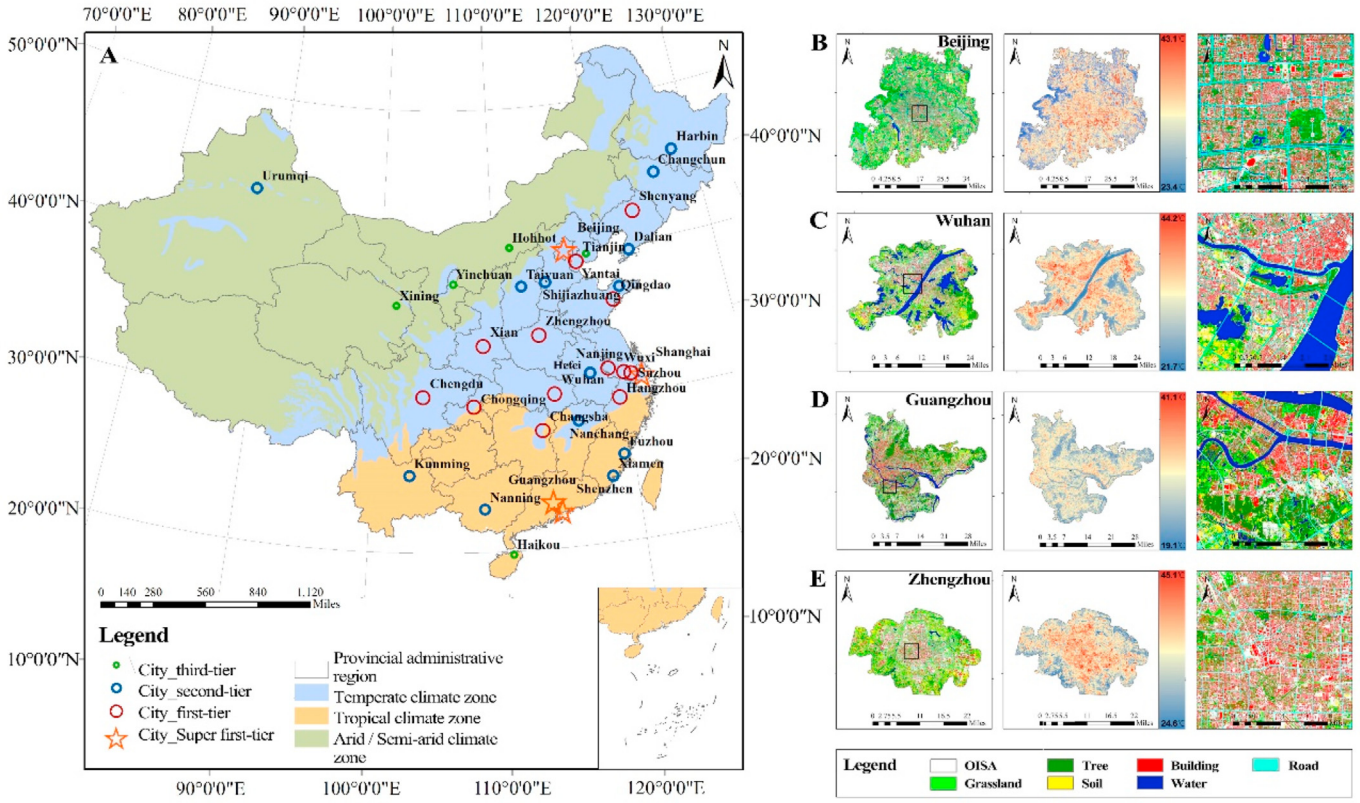

Fig. 2. (A): Locations of the 35 major cities in China, with the base map indicating the three climate zones of China. In addition, the circles with different sizes represent the cities at different development levels. (B)–(E): High resolution land cover mapping results of four representative cities: Beijing; Wuhan; Guangzhou; and Zhengzhou. The first column shows the high-resolution land cover maps, the second column shows the LST distribution maps, and the third column displays the details of the local areas delineated by the black frame in the first column.

resolution) (Huang et al., 2018; Huang and Wang, 2019). A total of 61 cloud-free ZY-3 images covering all 35 cities were acquired for the growing season (April to October) around 2015 to ensure consistent vegetation conditions. The processing flow is summarized as follows: Firstly, the MS images were registered to the PAN nadir image with a root-mean-square error (RMSE) of less than one pixel; then, Gram-Schmidt pan-sharpening was applied to fuse the MS images with the PAN nadir images, to improve their spatial resolution; finally, a series of ancillary datasets, including A-map, Map World, and Open Street Map (OSM), were used to help extract the land cover from the sharpened MS images after spatial registration.

Map World was the main source of water information, and it was also used as a supplement to A-map and OSM to obtain buildings and roads. After acquiring these three land-cover categories, they were used as a mask layer to the ZY-3 image. Then, using the random forest classifier, the rest of the image was classified into four other land-cover categories: grassland, tree, bare soil, and other impervious surface area (OISA, e.g., squares, open areas, pavements). In this research, we defined the land category of AS by merging the buildings, roads, and OISA. The overall accuracy based on 41,571 spatially independent validation samples was 88%, with the producer's accuracy and user's accuracy for all the land-cover classes exceeding 85%, implying a reliable mapping result. Please refer to Huang et al. (2020) for details of the mapping and accuracy assessment. In addition, to further understand the composition and spatial distribution of the land-cover types in these 35 cities, we calculated their total proportion and aggregation index for the subsequent analysis.

3.2. Urban area extraction

The urban area for each city was extracted by referring to the definition in Zhou et al. (2015). In detail, we first generated a building intensity (BI) map from the land-cover map of each city using a 1 × 1 km moving window. Subsequently, the BI map was divided into high- and low-intensity built-up patches with a threshold of 50%. The high-intensity built-up patches were then aggregated to obtain a compact urban area. The urban areas of the 35 cities range from 221.6 km^2 (Xiamen) to 3518.21 km^2 (Beijing). The final mapping results of four representative metropolises of China (Beijing, Wuhan, Guangzhou, and Zhengzhou) are shown in Fig. 2(B).

3.3. LST retrieval

To produce the LST distribution maps of the 35 cities, all of the Landsat 8 Surface Reflectance Tier 1 product (L8_SR) with cloud coverage less than 70% available between June and August during 2013–2018 were obtained from the United States Geological Survey (USGS). Detailed information about the images acquired for each city is presented in Table A.1. The L8_SR product is the atmospherically corrected surface reflectance from the Landsat 8 Operational Land Imager (OLI) with a spatial resolution of 30 m and thermal Infrared Sensor (TIRS) sensors with a resampled spatial resolution of 30 m. In addition, this product is made up of five visible and near-infrared (VNIR) bands and two short-wave infrared (SWIR) bands that have been processed to orthorectified surface reflectance, and two thermal infrared (TIR) bands that have been processed to orthorectified brightness temperature (USGS, 2013).

The cloud and cloud shadows in the images were filtered out according to the quality assessment (QA) band, and based on the Landsat Data Users Handbook Version 5.0 (NASA, 2019), the LST could then be retrieved through calculating a set of parameters:

$$\mathrm{LST} = \frac{T_B}{1 + (\lambda \times T_B/\rho)\ln \varepsilon} \quad (1)$$

where T_B is the orthorectified brightness temperature (Kelvin, K), obtained from the pixel values of L8_SR Band10 (the scale factor is 0.1); and λ is the wavelength of the radiation emission. The center wavelength (10.8 μm) of L8_SR Band10 was used. $\rho = \frac{(h \times c)}{\delta} = 1.438 \times 10^{-2} mK$, in which h is Planck's constant (6.626×10^{-34} J s), $c$is the speed of light (2.998×10^{8} m s^{-1}), and δ is the Boltzmann constant (1.381×10^{-23} J K^{-1}) (Peng et al., 2018). ε is the surface emissivity, whose values were determined by the normalized difference vegetation index (NDVI) (Defries and Townshend, 2007; Valor and Caselles, 1996).

In this research, the final LST distribution map for each city (Fig. 2(B)) was obtained by averaging all the LST distribution maps available during the selected period, for the following reasons: 1) the LST retrieved from a single-date image may be greatly affected by meteorological conditions (e.g., precipitation, wind speed, wind direction); and 2) the de-clouding processing for a single image often results in some missing LST values.

3.4. Investigation of the Veg-AS-LST relationship

A series of grid samples of 360 × 360 m were established within each city, and the composition of the trees, grassland, and AS was then acquired for each grid cell. The grid size, i.e., 360 × 360 m, was determined referring to Myint et al. (2010), achieving a trade-off between preservation of land-cover details and analysis of their effects on LST. By superimposing the grid layer upon the high-resolution land-cover and LST distribution maps, we could calculate the proportion of each land-cover type and the averaged LST for each grid cell sample. Please note that we focused our analysis on the so-called "pure grid cells", i.e., the ones containing only trees, grassland, and AS, to avoid the effects of other land-cover categories. The chosen grid samples were divided into 10 groups according to proportion gradients of AS, i.e., 0–10% (Group No. 1), 10%–20% (Group No. 2), … …, and 90–100% (Group No. 10), respectively. Fig. 3(A) illustrates the grouping results for the grid cell samples from Beijing as an example. Here, from the first group to the tenth group, we randomly selected a grid cell sample in each group to display the composition of the land cover, as shown in Fig. 3(B). We then further divided each group into 100 intervals with an increment of 0.1% AS. Since the number of grid cell samples in each interval may be different, we only took one of the grid samples, whose proportion of AS was the median of all the samples, as a representative of each interval (Fig. 3(C)). This ensured that the number of grid cell samples in each group was equal (i.e., the number of intervals, 100), which confirmed the inter-group comparability of the subsequent regression results.

A regression model was then established for each group, based on the grid cell samples in it. The proportions of Veg (tree or grassland) and AS were set as the independent variables, and the averaged LST was set as the dependent variable. For each model, the variable with the maximum regression coefficient was regarded as the dominant variable affecting LST. Since the grids only included trees, grassland, and AS, multicollinearity existed when the three independent variables were input into the regression model simultaneously. To alleviate the multicollinearity, the hierarchical regression model (HRM) (Lankau and Scandura, 2002) was adopted to separately analyze the tree-AS-LST relationship and the grassland-AS-LST relationship by controlling the third independent

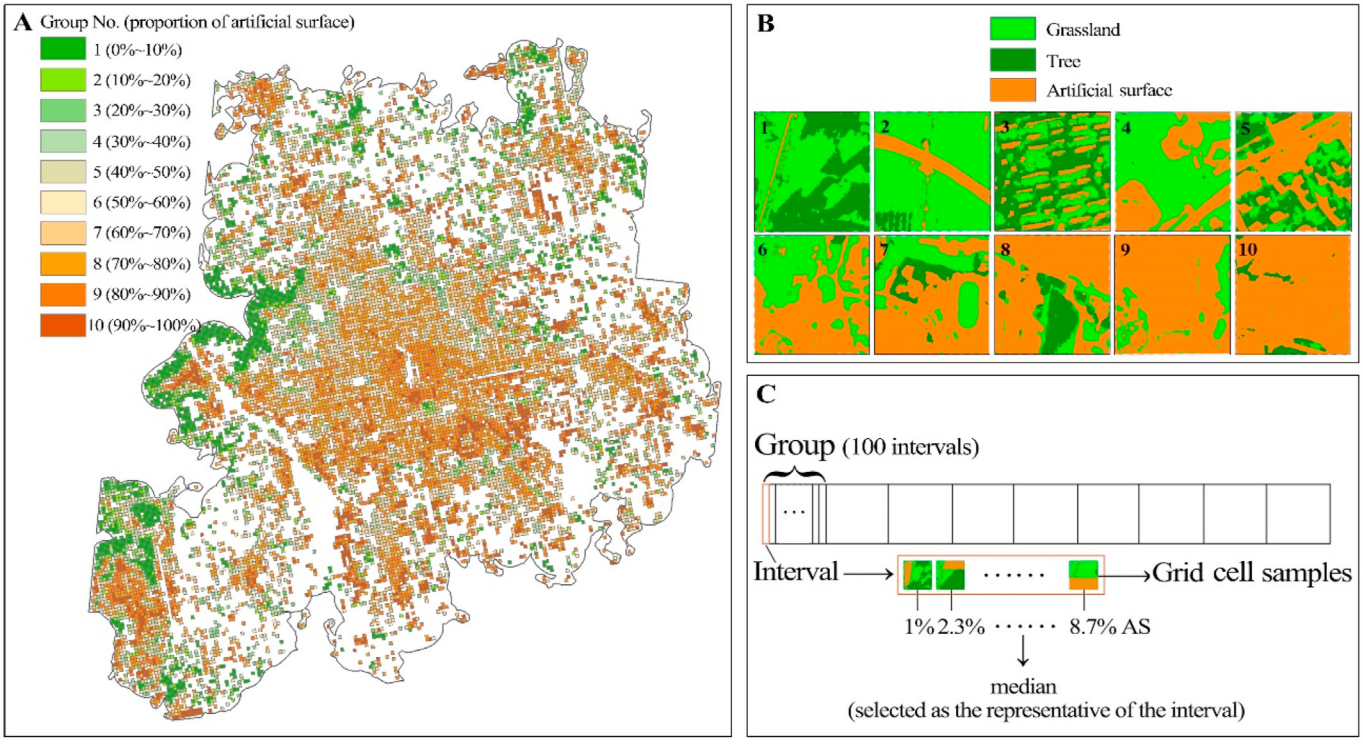

Fig. 3. An example of the grouping results for the grid cell samples from Beijing. (A): All the grid cell samples. (B): Random grid cell samples respectively selected from Group No. 1 to Group No. 10. (C): A graphical explanation of the groups, intervals, and grid cell samples.

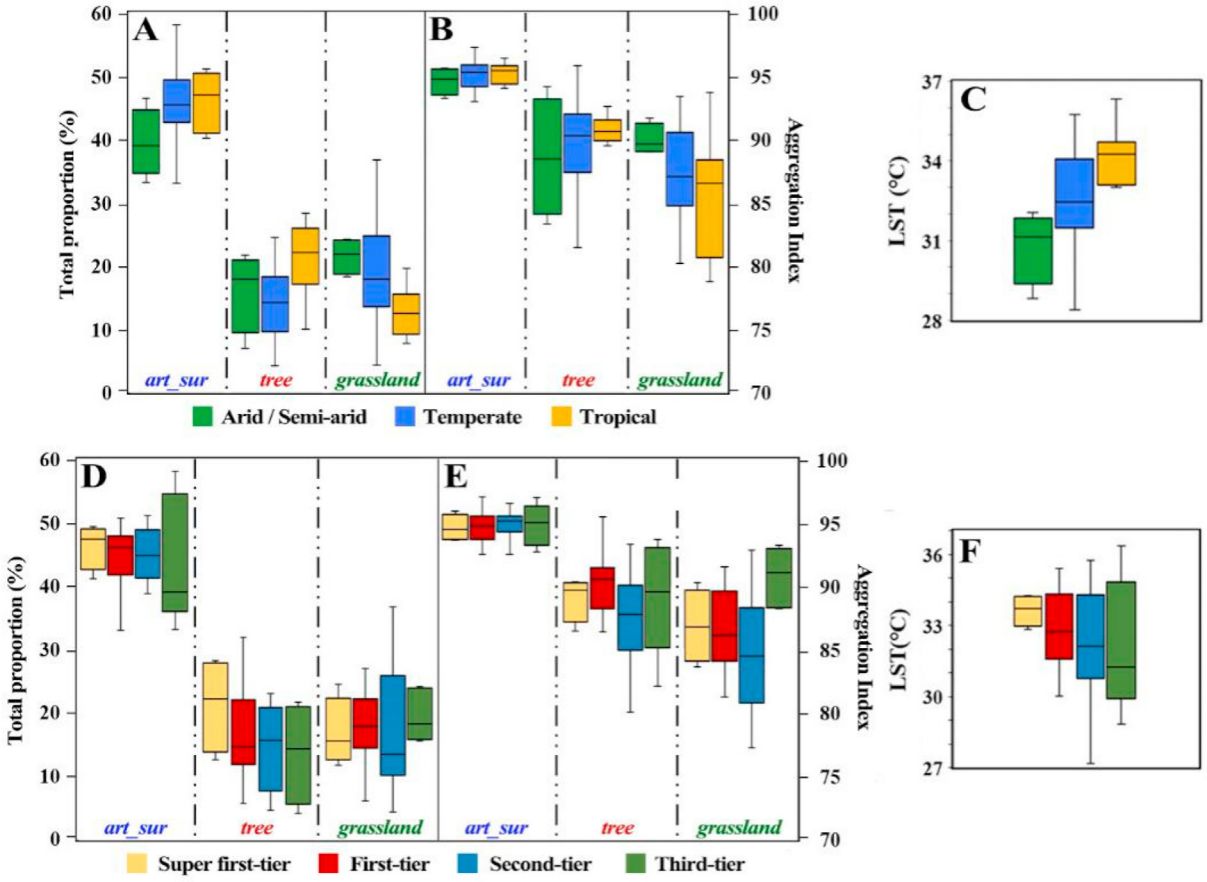

Fig. 4. Boxplots of the total proportions and aggregation index of AS, trees, and grassland, as well as the LST of cities in three climate zones ((A)–(C)) and four development levels ((D)–(F)). The horizontal lines (boxes and whiskers) from top to bottom in each boxplot are the maximum value, the 1st quartile (Q1), the median, the 3rd quartile (Q3), and the minimum value, respectively.

variable. HRM is a bi-layer linear regression model (Stephen and Anthony, 2002), whose first layer is composed of control variables and a dependent variable, and the second layer is built by adding independent variables using an "enter" method, as shown below:

$$LST_i = \alpha_i Veg_i + \beta_i AS_i + \varepsilon_i \quad (2)$$

where α_i is the coefficient of Veg (tree or grassland), β_i is the coefficient of AS, and ε_i is the intercept of Group No. i ($i = 1, 2, \ldots\ldots, 10$). Here, the regression coefficient measures the influence intensity of Veg and AS on LST. On the basis of the conceptual diagram in Fig. 1, when the proportion of AS is low (for example, in Group No. 1-No. N), if $\alpha_1 > \beta_1, \ldots\ldots, \alpha_N > \beta_N$, Veg is regarded as the dominant variable. Otherwise, when the proportion of AS is high (for example, in Group No. (N+1)-No. 10), if $\alpha_{N+1} < \beta_{N+1}, \ldots\ldots, \alpha_{10} < \beta_{10}$, AS is considered as the dominant variable. On this condition, 10*N% is the turning point of AS for this city.

4. Results

4.1. Characteristics of the AS, Veg, and LST in the 35 major cities of China

As presented in Table A.2, the total proportions (Prop_Total) and aggregation index (AI) values of AS, trees, and grassland in 35 major cities of China, as well as the LST values, were calculated at the city scale, and the results were further grouped by climate zones and development levels (Fig. 4). Among these cities, the Prop_Total of AS, trees, and grassland vary from 33.05% (Chengdu, CD) to 58.01% (Tangshan, TS), 4.14% (TS) to 31.92% (Shenyang, SY), and 4.35% (Taiyuan, TY) to 36.67% (Hefei, HF), respectively, and the AI varies from 93.00% (Chongqing, CQ) to 97.26% (Suzhou, SuZ), 81.41% (TY) to 95.78% (SuZ), and 78.75% (Kunming, KM) to 93.69% (Haikou, HK), respectively. The LST across the cities ranges from 27.16 ± 5.09 °C (KM) to 36.35 ± 2.38 °C (HK).

Fig. 4(A) shows that the Prop_Total of AS and trees in the tropical cities are 45.81% ± 4.26% and 21.20% ± 5.55%, respectively, which is higher than the temperate (45.52% ± 4.97% and 14.32% ± 6.48%) and arid/semi-arid (39.35% ± 4.72% and 16.08% ± 5.53%) cities, while the Prop_Total of grassland in the arid/semi-arid cities is 21.54% ± 2.45%, which is higher than that in the tropical (12.90% ± 3.69%) and temperate (19.12% ± 7.51%) cities. Similar results can be observed in the AI (Fig. 4(B)). The AS and trees in the tropical cities (95.22 ± 0.80 and 89.92 ± 1.02) are the most aggregated, followed by the temperate (95.17 ± 1.20 and 89.76 ± 3.35) and arid/semi-arid (94.59 ± 1.09 and 88.56 ± 4.70) cities. In contrast, the grassland is more intensively distributed in the arid/semi-arid (89.98 ± 1.22) cities than in the temperate (87.50 ± 3.58) and tropical (85.71 ± 4.90) cities. In addition, the mean LST in the tropical cities is, respectively, 1.05 °C and 2.86 °C higher than in the temperate and arid/semi-arid cities (Fig. 4(C)). The results indicate that, due to the warm and humid background climate, the tropical cities correspond to more massive and concentrated AS and trees compared to the cities with arid/semi-arid climates in China.

Fig. 4(D) shows that the Prop_Total of AS and trees are obviously higher in the cities at higher development levels. Moreover, it is worth noting that, in the super first-tier cities, the AI of AS is

relatively low (Fig. 4(E)), whereas that of trees and grassland is high, which indicates that targeted vegetation planting has been implemented in these areas, to avoid overly dense urban construction. However, the mean LST of the developed cities is still higher than that of the other cities (Fig. 4(F)). This can be mainly attributed to the crowded population and various anthropogenic activities that lead to high heat emissions, such as industrial production, domestic discharge, and commercial trade (Jia and Zhao, 2019).

The proportion of Veg (trees/grassland) and the corresponding LST along the proportion gradients of AS inside the 35 major cities are shown in Fig. 5. It can be observed that, with the increase of the proportion of AS, the proportion of trees and grassland in most cities shows a non-linear decrease, while in some cities (e.g., CC, HH, and SJZ) a linear decline can be seen. However, for some southeast coastal cities, e.g., GZ, HK, HZ, NJ, SZ, SuZ, WX, and YT, the curve for grassland shows a slight rise in some areas that are covered by 10–30% AS, which may be the result of urban planning and management. On the other hand, the LST of most cities (except HZ, TJ, UQ, XN) shows a linear positive relationship with the proportion of AS.

4.2. Joint effects of Veg and AS on LST

Fig. 6(A) and (B) display the overall HRM results for the 35 cities. With the increment in the AS proportion, the impact of trees and grassland on LST gradually weakens, and the impact of AS is slowly enhanced, which is consistent with the findings of previous research (Estoque et al., 2017; Ziter et al., 2019). It is clear that AS and Veg exhibit a competitive effect on LST: when the proportion of AS is low, the impact of Veg on LST is stronger than that of AS; and as the proportion of AS increases to a certain threshold (i.e., the turning point), AS replace Veg as the land-cover class having the dominant effect on LST. Results verify the assumption proposed in this study. For trees, the turning point appears at 70% AS (Fig. 6(C), $R^2 = 0.43$, $p < 0.05$). With respect to grassland, the turning point appears at 60% AS (Fig. 6(D), $R^2 = 0.38$, $p < 0.05$).

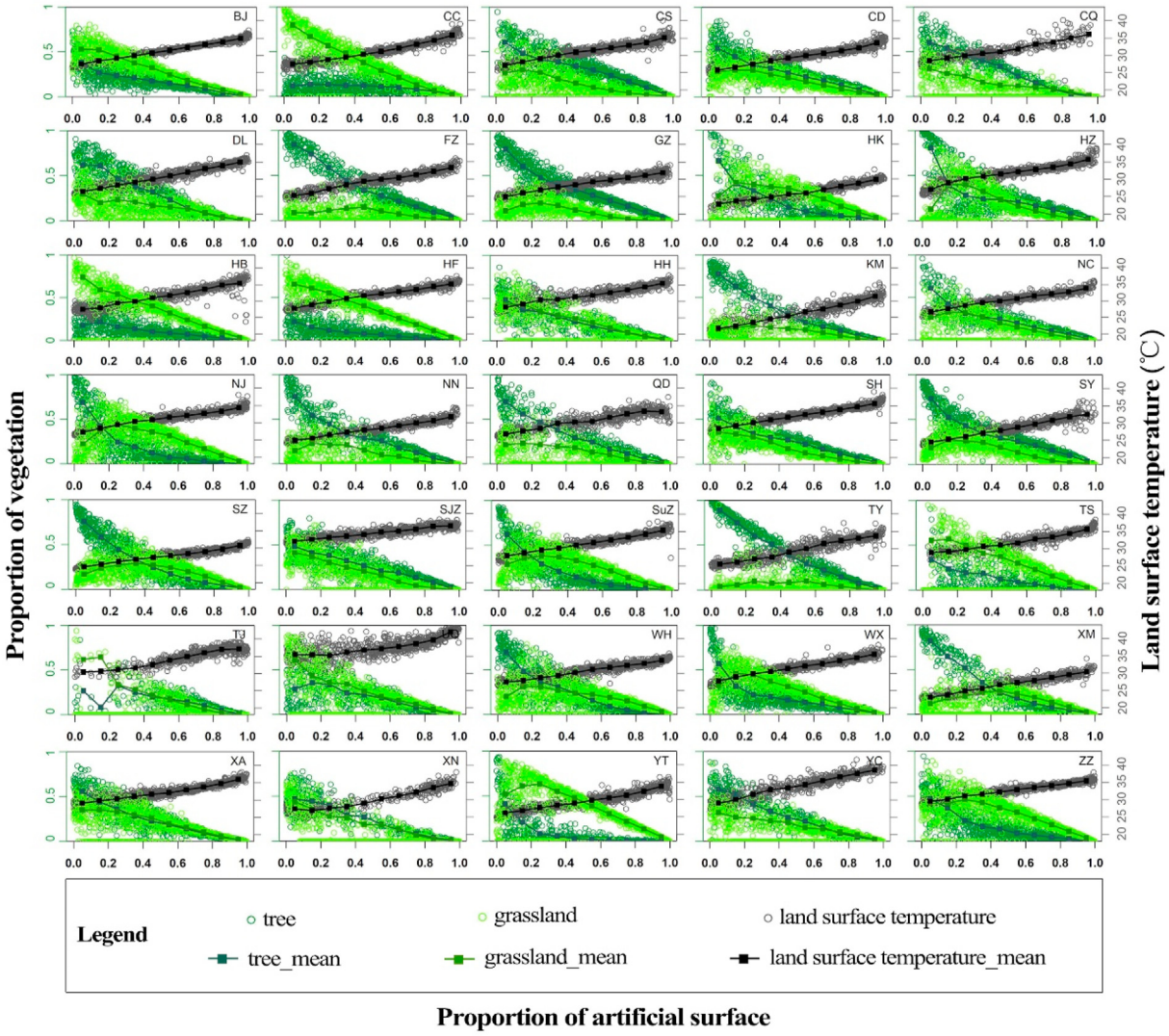

Fig. 5. The proportion of trees and grassland and the averaged LST in each grid cell sample along the proportion gradients of AS within urban areas of the 35 cities. The circles represent the value of the grid cell sample in each interval, and the squares represent the average values of the samples in each group. BJ (Beijing), CC (Changchun), CS (Changsha), CD (Chengdu), CQ (Chongqing), DL (Dalian), FZ (Fuzhou), GZ (Guangzhou), HB (Harbin), HF (Hefei), HH (Hohhot), HK (Haikou), HZ (Hangzhou), KM (Kunming), NC (Nanchang), NJ (Nanjing), NN (Nanning), QD (Qingdao), SH (Shanghai), SJZ (Shijiazhuang), SuZ (Suzhou), SY (Shenyang), SZ (Shenzhen), TJ (Tianjin), TS (Tangshan), TY (Taiyuan), UQ (Urumqi), WH (Wuhan), WX (Wuxi), XA (Xi'an), XM (Xiamen), XN (Xining), YC (Yinchuan), YT (Yantai), ZZ (Zhengzhou).

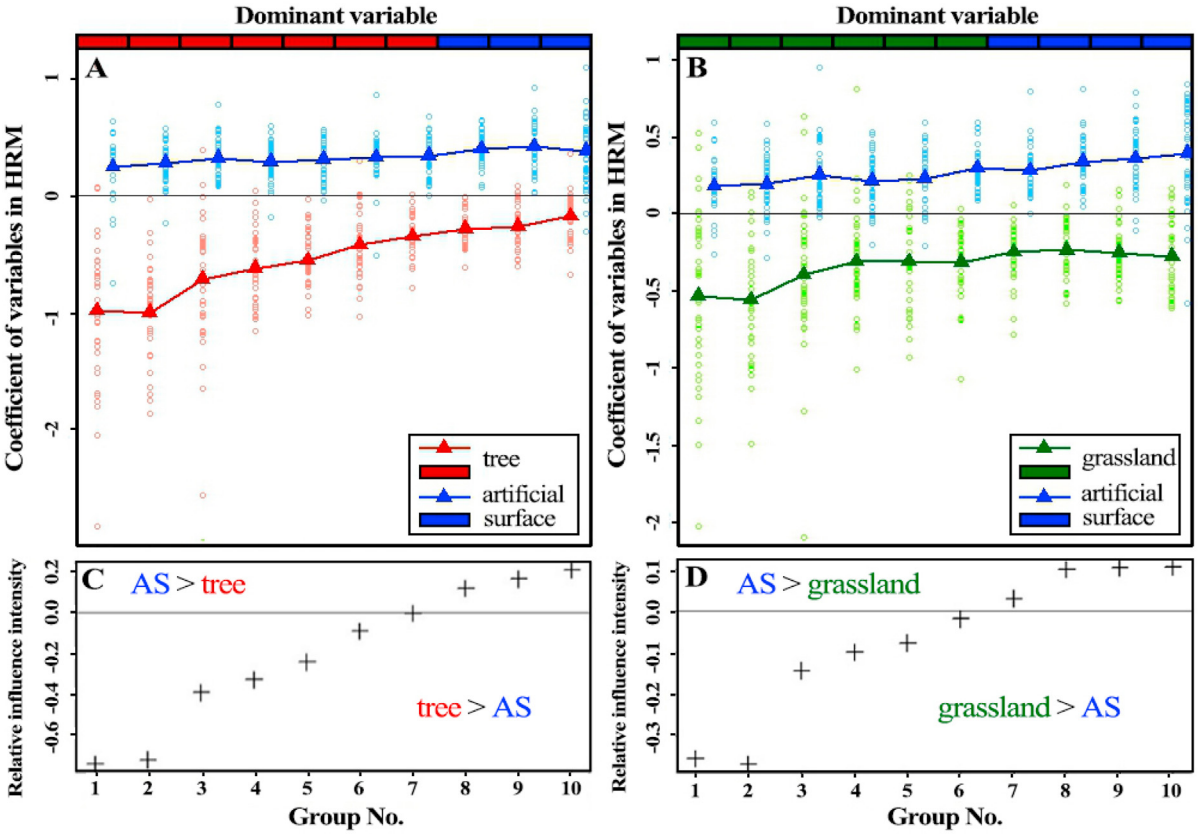

Fig. 6. Overall results for the 35 cities and the dominant variable in each group. (A)–(B): The HRM results for trees (or grassland) and AS. (C)–(D): The relative intensity of the influence of trees (or grassland) and AS on LST. The hollow circle represents the regression coefficient for each single city, and the solid triangles represent the mean of the regression coefficients for all the cities. Group Nos. 1 to 10 represent the proportion of AS between 0 and 10%, 10–20%, 20–30%, 30–40%, 40–50%, 50–60%, 60–70%, 70–80%, 80–90%, and 90–100%, respectively. In the bar chart above the figure, the red, dark green, and blue indicate that tree, grassland, and AS is the dominant variable in this group, respectively.

4.3. Turning points for cities in different climate zones and development levels

The trends of the HRM coefficients along the proportion gradients of AS in three climate zones (Fig. 7) and four development levels (Fig. 8) are similar to the overall results for the 35 cities (Fig. 6). Although there are fluctuations in the results for the arid/semi-arid cities and the third-tier cities, which may be related to their limited number, the competition phenomenon and turning points still exist.

For cities located in arid/semi-arid, temperate, and tropical regions, the turning points of AS for trees are 90% (Fig. 7(A), $R^2 = 0.28$, $p < 0.05$), 60% (Fig. 7(B), $R^2 = 0.56$, $p < 0.05$), and 60% (Fig. 7(C), $R^2 = 0.45$, $p < 0.05$), respectively, and the turning points of AS for grassland are 90% (Fig. 7(D), $R^2 = 0.19$, $p < 0.05$), 50% (Fig. 7(E), $R^2 = 0.49$, $p < 0.05$), and 50% (Fig. 7(F), $R^2 = 0.46$, $p < 0.05$), respectively. With respect to the different city ranks, i.e., the super first-tier, first-tier, second-tier, and third-tier cities, the turning points of AS for trees are 60% (Fig. 8(A), $R^2 = 0.36$, $p < 0.05$), 70% (Fig. 8(B), $R^2 = 0.47$, $p < 0.05$), 70% (Fig. 8(C), $R^2 = 0.49$, $p < 0.05$), and 70% (Fig. 8(D), $R^2 = 0.40$, $p < 0.05$), respectively, and for grassland, the turning points of AS are 50% (Fig. 8(E), $R^2 = 0.31$, $p < 0.05$), 50% (Fig. 8(F), $R^2 = 0.41$, $p < 0.05$), 60% (Fig. 8(G), $R^2 = 0.43$, $p < 0.05$), and 70% (Fig. 8(H), $R^2 = 0.37$, $p < 0.05$), respectively.

5. Discussion

5.1. Significance and implications of the turning point

It has been widely reported that Veg plays a cooling role in cities, by evaporating, storing carbon dioxide (CO_2), and providing shade (Oke, 1989). In contrast, areas covered by AS generally exhibit higher LST than other areas because the impervious urban materials used in AS do not retain water for evaporation and absorb heat rapidly when exposed to solar radiation (Yuan and Bauer, 2007). During the process of urbanization, AS gradually replace Veg as the most prevalent land cover in urban areas due to the construction of infrastructure and deforestation (Qiao et al., 2013), which changes the surface albedo, alters the efficiency of heat absorption and dissipation and elevates CO_2 emissions, leading to UHI (Bowler et al., 2010).

To offset the heat emissions, China has made great efforts in greening cities (Zhao et al., 2016). How to achieve a trade-off and compromise between the need of AS construction for urban development and the urgency of Veg planting for climate adaption is paid close attention by those decision-makers. It is on the basis of both land allocation and temperature regulation that this study assumes and obtains the turning point between AS and Veg for their competitive effect on LST. Compared with the thresholds obtained in previous studies, the turning point can reflect how the

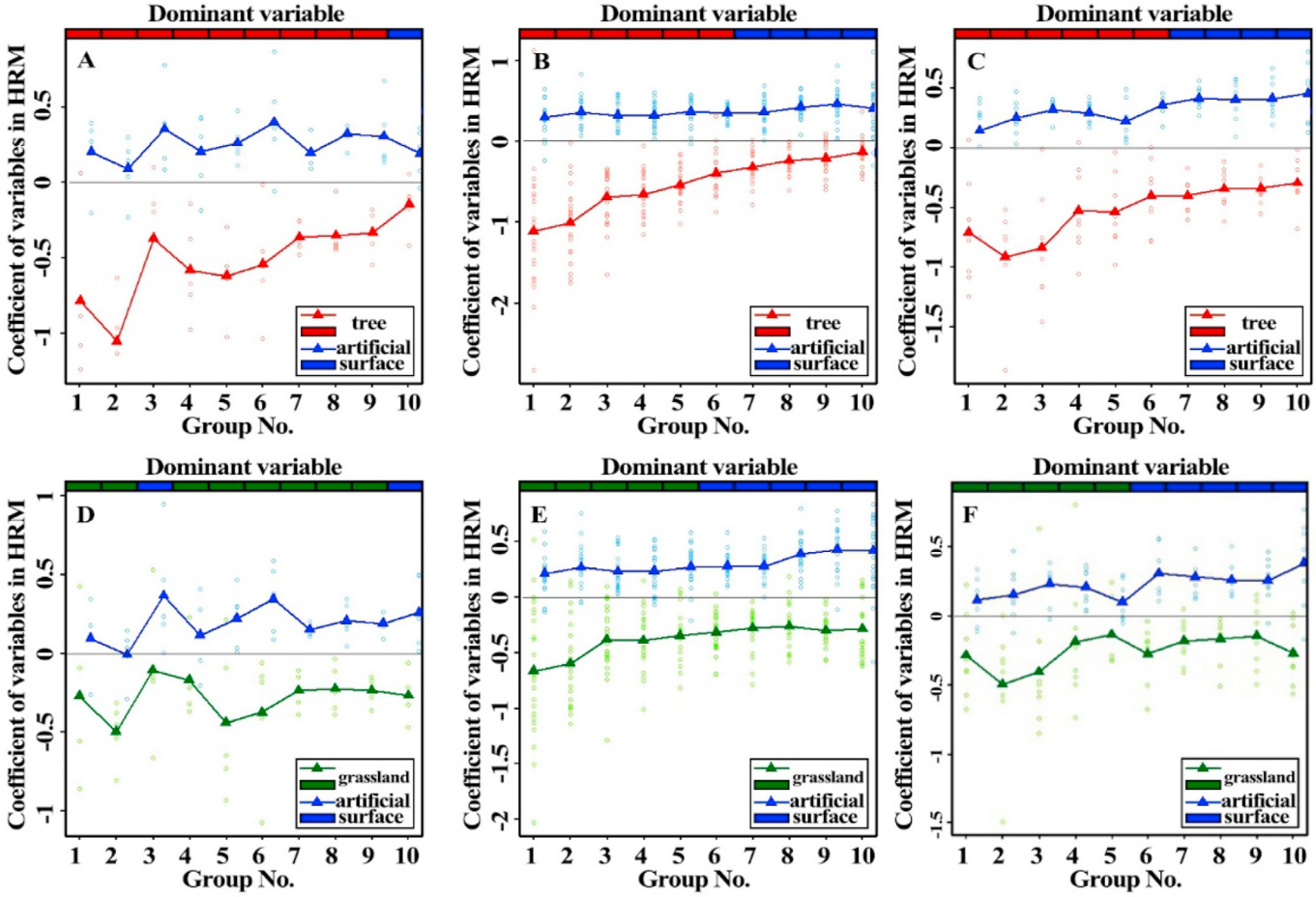

Fig. 7. The HRM results for cities in the arid/semi-arid climate zone ((A), (D)), temperate climate zone ((B), (E)), and tropical climate zone ((C), (F)), respectively. (A)–(C): tree-AS-LST relationship; (D)–(F): grassland-AS-LST relationship.

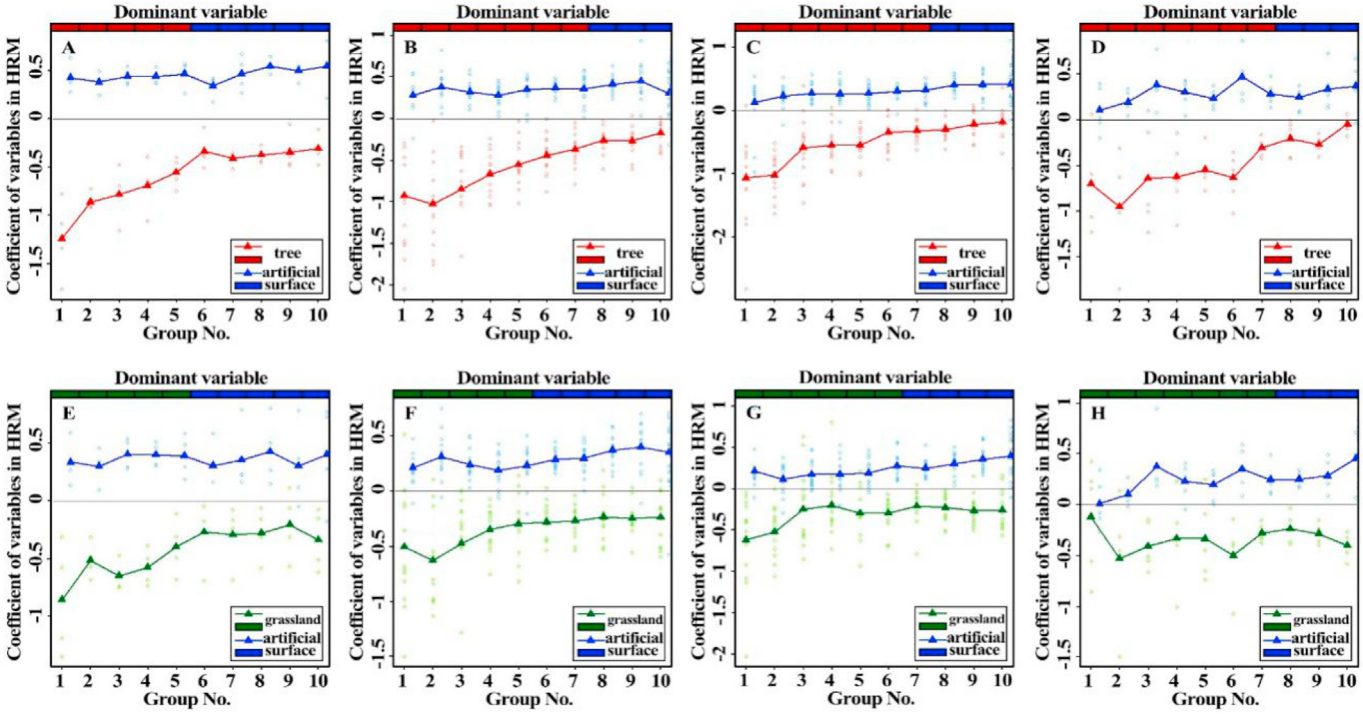

Fig. 8. The HRM results for the super first-tier cities ((A), (E)), first-tier cities ((B), (F)), second-tier cities ((C), (G)), and third-tier cities ((D), (H)), respectively. (A)–(D): tree-AS-LST relationship; (E)–(H): grassland-AS-LST relationship.

urban LST responds to the different relative proportions of Veg to AS, rather than a single land cover category, so as to better manifest the dynamic thermal changes under the complex interaction between land covers.

The existence of the turning point with regard to the proportion of AS has important implications for urban management. For instance, it could be regarded as the "warning level" for the proportion of AS within urban areas. According to the results of this study, in areas covered by AS exceeding 60% or 70%, some targeted measures such as optimizing the spatial pattern of the AS may be needed to compensate for the lack of vegetation cooling capacity. It is true that the increase of AS is inevitable during socio-economic development, but the in-depth understanding of the joint effect of land covers on LST will sound the alarm for intensive construction, and knowledge of the turning point will facilitate to prevent the further rise of summer daytime LST.

Our findings on turning point further reveal that the work towards urban climate adaptation in different regions needs to be elaborately designed in combination with their climatic and developmental peculiarity. For cities with mild and humid climate, improving vegetation (especially trees) coverage is preferred as a primary means of cooling, while for cities at higher development level, it is a more effectual and practicable strategy to consume the abundant anthropogenic heat emissions by using permeable pavement materials (Li et al., 2014), increasing the vegetation connectivity (Maimaitiyiming et al., 2014) and their vertical coverage (e.g., green wall and green facades) (Koc et al., 2018), and scattering the distribution of high-rise buildings (Huang and Wang, 2019), given their limited planting space.

Moreover, it can be noticed that the turning point is different for trees (70%) and grassland (60%), which signifies that, in the competition with AS, the cooling effect of urban trees is stronger than that of urban grassland in the summer daytime. Myint et al. (2015) observed a similar phenomenon in Las Vegas and Phoenix in the southwestern U.S. Compared with grassland, the surface roughness (Miranda et al., 1997), rooting depth (Jackson et al., 1997), and leaf area index (LAI) of trees are usually higher, so their cooling capability is stronger under the same climatic environment. Several studies have shown that the transition of taller woody vegetation (e.g., trees) to grassland increases air temperature and LST in tropical regions (Lee et al., 2011), whereas when the transition is from grassland to trees, continuous cooling is observed throughout the season (Abera et al., 2019). Therefore, for the sake of maximizing the cooling efficiency of vegetation in summer daytime, prioritizing tree planting in planning urban green landscapes will be a better choice.

5.2. Influencing factors of the turning point

Land cover conversions change the biophysical properties (e.g., CO_2, albedo, etc.) of land surface in urban areas. These surface properties correspond to albedo-related radiative forcing and carbon sequestration potential, which are the primary factors affecting the LST. In the study of Stéfanon et al. (2012), the effects of albedo and CO_2 on LST were found to be obviously different in each climatic zone. Similar phenomenon was also verified along the urbanization intensity gradients (Trlica et al., 2017). Therefore, this study mainly discusses the influencing factors of turning point from the aspects of background climate and urban development level.

Background climate of a city determines its local land use patterns and major vegetation types. It can be observed that the turning points for cities in colder and drier regions (arid/semi-arid climate zones) are higher than those in hotter and wetter regions (temperate and tropical climate zones), for both trees and grassland. Higher turning points implies that less Veg is needed to offset the AS-induced heat. On the one hand, the heat mitigation ability of urban Veg in arid regions is higher. This can be explained in two respects. Firstly, in summer, plants in the arid zone, especially shallow-rooted grassland, are more resistant to a prolonged drought environment (Stéfanon et al., 2012; Wu et al., 2019). In contrast, the Veg in temperate and tropical cities suffers more losses induced by drought and high temperatures, which weakens its cooling efficiency. Secondly, the high illumination and low humidity in arid climate zones provide favorable conditions for the evapotranspiration of Veg (Yu et al., 2018). On the other hand, compared to tropical cities near the equator, the AS in arid cities receives shorter duration and lower intensity of solar radiation, so it has lower heating potential in summer daytime. Moreover, in China, the arid/semi-arid climate zones are exclusively located in sparsely populated areas, so the anthropogenic heat emissions in these regions are relatively less.

The level of urban development is directly related to the land use pattern and the carbon emissions. As reported in the literature, high-density urban areas tended to have lower albedo, higher AS coverage, less Veg fraction, and higher LST (Trlica et al., 2017; Yue et al., 2019). In turn, as urban develops, the deterioration of the thermal environment further increases the energy consumption (e.g., air conditioners, refrigerators, etc.) in summer (Hirano and Fujita, 2012). Such a vicious cycle contributes to the higher heat emissions per unit area in developed cities than in less-developed ones. Our findings consolidate this phenomenon from the turning point perspective: the higher the development level of a city, the lower the turning point, which means even a relatively low AS coverage is capable of elevating the LST significantly in developed cities compared to less-developed ones. In the case of super first-tier cities, for example, when the proportion of AS exceeds 60% or 50%, the warming effect is stronger than the cooling effect of trees or grassland.

5.3. Importance of the high-resolution remote sensing data

Based on satellite-derived data of various spatial resolutions, ranging from sub-meter to 1 km, the effect of Veg or AS on LST has been widely investigated. The Advanced Very High Resolution Radiometer (AVHRR) and the Moderate Resolution Imaging Spectroradiometer (MODIS) are the major data sources for global, national, and regional analysis (e.g., Peng et al. (2014) and Wu et al. (2019)). Medium-resolution remote sensing data (e.g., Landsat, Advanced Spaceborne Thermal Emission and Reflection Radiometer (ASTER)) are employed more often in the case studies of single cities or urban agglomerations (e.g., Cao et al. (2010)). In addition, through calculating the NDVI from the bands of Landsat 5 Thematic Mapper (TM) or Landsat 7 Enhanced Thematic Mapper Plus (ETM+) images, a number of studies (Dousset and Gourmelon, 2003; Weng, 2009; Estoque et al., 2017) have established a negative linear or non-linear LST-Veg relationship in different cities, including Los Angeles (USA), Paris (France), Indianapolis (USA), Twin Cities (USA), Pearl River Delta (China), Bangkok (Thailand), Jakarta (Indonesia), and Manila (Philippines).

A common problem with the widely used low- and medium-resolution remote sensing imagery is that they are too coarse to accurately capture detailed information about land cover within cities, leading to an insufficient understanding and even misunderstanding of their ecological function (Nelson et al., 2009; Pickett, 2010). A study by Li et al. (2013) showed that, although the correlation between LST and green space coverage is consistently negative across resolutions (i.e., QuickBird, 2.44 m; SPOT, 10 m; and Landsat TM, 30 m), the green spaces seemingly show a stronger cooling effect at finer spatial resolutions. Moreover, subject to the limited spatial resolution, utilizing the NDVI or a generalized

concept of "green spaces" as a whole to describe urban Veg cannot reveal the difference between vegetation species, with regard to their effect on LST. This stresses the requirement for a finer-scale analysis with high-resolution RS data. Compared to those coarse-grained studies, our results divide the urban Veg into trees and grasslands to investigate their respective cooling capability, and finely depicts their distribution along the proportion gradient of AS, which is of essence for us to understand the spatial coherence between thermal environment and detailed urban land covers.

5.4. Limitations and uncertainties

Some limitations remain in this study. Although we have chosen pure samples in the experiments, other land-cover types adjacent to Veg and AS can also impact LST, to some extent, as heat flows in the space and radiates into the surroundings, leading to a few abnormal results. For example, the suburbs of the cities of TJ and XM are adjacent to a large area of bare soil and water (Fig. A1), respectively, which may be the main cause of the positive coefficients of the trees in TJ and the negative coefficients of the AS in XM in the first and second groups (Fig. A2, Fig. A3). Considering that the establishment of HRM requires enough number of grid samples, so those samples close to water and bare soil are not completely eliminated. Nonetheless, at the city scale, the open water fraction does not appear to show strong influence on the overall conclusion of this study.

Besides, given the lack of vegetation height information, this study did not quantitatively discuss the joint effect of AS and Veg on LST in the vertical space. Relevant research will be strengthened as the data continues to improve in future.

6. Conclusions

Vegetation (Veg) and artificial surfaces (AS) are the predominant land-cover types in urban areas. Although they have been manifested to be crucial for regulating the urban microclimate and controlling the thermal cycling between the land surface and the lower atmosphere in numerous literature, to date, the research on Veg-AS-LST relationship fails to answer two questions. First, how does AS and Veg with different composition interact to affect LST? Second, how does this effect vary in different geographic locations? Accordingly, this study attempted to address these issues through satellite observation and the statistical modeling.

Our results reveal that: 1) The Veg composition (the proportions of trees and grassland) and its spatial distribution along the proportion gradient of AS shows significant regional differences, which are related to the background climate and urban planning. 2) The Veg-induced cooling and the AS-induced warming show competitive effect on LST, and their proportion determines which one is dominant. 3) The general results for the 35 major cities of China indicated that when the proportion of AS reaches the turning point of 70% (60%), respectively, its warming effect on LST is stronger than the cooling effect of trees (grassland). It was also found that, in most cities, trees are a stronger cooling source than grassland. 4) The turning points for cities at higher development levels are lower, which suggests that even a low AS coverage (~50–60%) in these areas can lead to an increase in LST. 5) Compared to cities in temperate and tropical climate zones, urban Veg in the arid/semi-arid zone exhibits a better performance in heat mitigation (i.e., a higher turning point).

These findings fill the gaps in understanding the joint effects of Veg and AS on LST from the perspective of their competitive relationship, and further move forward in quantitatively estimating the turning points for all 35 major cities of China. This systematic and reliable research based on high-resolution LULC data across multiple cities is not only instrumental to summarizing the general pattern of such joint effect in most regions, but better reflects their trends in different climatic zones and their relationship with urban development levels. In the context of global urban warming, the turning points we have obtained are of practical significance for guiding urban landscape planning and promoting the construction of healthy urbanization.

CRediT authorship contribution statement

Yue Liu: Conceptualization, Methodology, Software, Validation, Formal analysis, Writing - original draft. **Xin Huang:** Conceptualization, Resources, Writing - review & editing, Supervision, Funding acquisition. **Qiquan Yang:** Conceptualization, Formal analysis, Writing - review & editing. **Yinxia Cao:** Resources, Data curation.

Declaration of competing interest

The authors declare that they have no known competing financial interests or personal relationships that could have appeared to influence the work reported in this paper.

Acknowledgement

The research was supported by the National Natural Science Foundation of China under Grants 41771360 and 41971295, and the CAS Interdisciplinary Innovation Team under Grant JCTD-2019-04.

Appendix A. Supplementary data

Supplementary data to this article can be found online at https://doi.org/10.1016/j.jclepro.2021.126034.

References

Abera, T.A., Heiskanen, J., Pellikka, P., Rautiainen, M., Maeda, E.E., 2019. Clarifying the role of radiative mechanisms in the spatio-temporal changes of land surface temperature across the Horn of Africa. Remote Sens. Environ. 221, 210–224.
Alavipanah, S., Wegmann, M., Qureshi, S., Weng, Q., Koellner, T., 2015. The role of vegetation in mitigating urban land surface temperatures: a case study of Munich, Germany during the warm season. Sustainability 7, 4689–4706.
Bowler, D.E., Buyung-Ali, L., Knight, T.M., Pullin, A.S., 2010. Urban greening to cool towns and cities: a systematic review of the empirical evidence. Landsc. Urban Plann. 97, 147–155.
Cao, X., Onishi, A., Chen, J., Imura, H., 2010. Quantifying the cool island intensity of urban parks using ASTER and IKONOS data. Landsc. Urban Plann. 96, 224–231.
Carleton, T.A., Hsiang, S.M., 2016. Social and economic impacts of climate, 2019 Science 353, 6304.
China Business Network Co., Ltd, 2019. https://www.yicai.com/news/100200 192.html.
Defries, R.S., Townshend, J.R.G., 2007. NDVI-derived land cover classifications at a global scale. Int. J. Rem. Sens. 15, 3567–3586.
Dousset, B., Gourmelon, F., 2003. Satellite multi-sensor data analysis of urban surface temperatures and landcover. ISPRS J Photogramm 58, 43–54.
Estoque, R.C., Murayama, Y., Myint, S.W., 2017. Effects of landscape composition and pattern on land surface temperature: an urban heat island study in the megacities of Southeast Asia. Sci. Total Environ. 577, 349–359.
Hirano, Y., Fujita, T., 2012. Evaluation of the impact of the urban heat island on residential and commercial energy consumption in Tokyo. Energy 37, 371–383.
Huang, X., Wang, Y., 2019. Investigating the effects of 3D urban morphology on the surface urban heat island effect in urban functional zones by using high-resolution remote sensing data: a case study of Wuhan, Central China. ISPRS J Photogramm 152, 119–131.
Huang, X., Chen, H., Gong, J., 2018. Angular difference feature extraction for urban scene classification using ZY-3 multi-angle high-resolution satellite imagery. ISPRS J Photogramm 135, 127–141.
Huang, X., Wang, Y., Li, J.Y., Chang, X.Y., Cao, Y.X., Xie, J.F., Gong, J.Y., 2020. High-resolution urban land-cover mapping and landscape analysis of the 42 major cities in China using ZY-3 satellite images. Sci. Bull. 65 (12), 1039–1048.
Jackson, R., Mooney, H.A., Schulze, E.D., 1997. A global budget for fine root biomass, surface area, and nutrient contents. Proc. Natl. Acad. Sci. U. S. A. 94 (14), 7362–7366.
Jia, W., Zhao, S., 2019. Trends and drivers of land surface temperature along the urban-rural gradients in the largest urban agglomeration of China. Sci. Total

Environ. 711, 134579.
Koc, C.B., Osmond, P., Peters, A., 2018. Evaluating the cooling effects of green infrastructure: a systematic review of methods, indicators and data sources. Sol. Energy 166, 486–508.
Lankau, M.J., Scandura, T.A., 2002. An investigation of personal learning in mentoring relationships: content, antecedents, and consequences. Acad. Manag. J. 45 (4), 779–790.
Lee, X., et al., 2011. Observed increase in local cooling effect of deforestation at higher latitudes. Nature 479, 384–387.
Li, H., Harvey, J., Ge, Z., 2014. Experimental investigation on evaporation rate for enhancing evaporative cooling effect of permeable pavement materials. Construct. Build. Mater. 65, 367–375.
Li, X., Zhou, W., Ouyang, Z., 2013. Relationship between land surface temperature and spatial pattern of greenspace: what are the effects of spatial resolution? Landsc. Urban Plann. 114, 1–8.
Maimaitiyiming, M., Abduwasit, G., Tashpolat, T., et al., 2014. Effects of green space spatial pattern on land surface temperature: implications for sustainable urban planning and climate change adaptation. ISPRS J Photogramm 89, 59–66.
Miranda, A.C., et al., 1997. Fluxes of carbon, water and energy over Brazilian cerrado: an analysis using eddy covariance and stable isotopes. Plant Cell Environ. 20 (3), 315–328.
Moriyama, M., Tanaka, T., Iwasaki, M., 2009. The Mitigation of UHI Intensity by the Improvement of Land Use Plan in the Urban Central Area: Application to Osaka City, Japan. In Second International Conference on Countermeasures to Urban Heat Islands (SICCUHI). Lawrence Berkeley National Laboratory, Berkeley, CA.
Myint, S.W., Brazel, A., Okin, G., Buyantuyev, A., 2010. Combined effects of impervious surface and vegetation cover on air temperature variations in a rapidly expanding desert city. GIScience Remote Sens. 47, 301–320.
Myint, S.W., Zheng, B., Talen, E., et al., 2015. Does the spatial arrangement of urban landscape matter? examples of urban warming and cooling in phoenix and las vegas. Ecosys. Health Sustain. 1, 1–15.
Nasa, 2019. Landsat 8 data users Handbook. http://landsathandbook.gsfc.nasa.gov/.
Nelson, M.D., McRoberts, R.E., Holden, G.R., Bauer, M.E., 2009. Effects of satellite image spatial aggregation and resolution on estimates of forest land area. Int. J. Rem. Sens. 30, 1913–1940.
Ng, E., Chen, L., Wang, Y., Yuan, C., 2012. A study on the cooling effects of greening in a high-density city: an experience from Hong Kong. Build. Environ. 47, 256–271.
Oke, T.R., 1989. The micrometeorology of the urban forest. Philos T R SOC B 324 (1223), 335–349.
Olson, D.M., et al., 2001. Terrestrial ecoregions of the world: a new map of life on earth. Bioscience 51, 933.
Peng, J., Jia, J., Liu, Y., Li, H., Wu, J., 2018. Seasonal contrast of the dominant factors for spatial distribution of land surface temperature in urban areas. Remote Sens. Environ. 215, 255–267.
Peng, S.S., Piao, S.L., Zeng, Z.Z., et al., 2014. Afforestation in China cools local land surface temperature. Proc. Natl. Acad. Sci. U. S. A. 111, 2915–2919.
Pickett, S.T.A., Kolasa, J., Jones, C.G., 2010. Ecological Understanding: the Nature of Theory and the Theory of Nature. Elsevier.
Qiao, Z., Tian, G., Xiao, L., 2013. Diurnal and seasonal impacts of urbanization on the urban thermal environment: a case study of beijing using modis data. ISPRS J Photogramm 85, 93–101.
Santamouris, M., Kolokotsa, D., 2015. On the impact of urban overheating and extreme climatic conditions on housing, energy, comfort and environmental quality of vulnerable population in Europe. Energy Build. 98, 125–133.
Shahmohamadi, P., Che-Ani, A.I., Etessam, I., Maulud, K.N.A., Tawil, N.M., 2011. Healthy environment: the need to mitigate urban heat island effects on human health. Procedia Eng 20, 61–70.
Stéfanon, M., Drobinski, P., d'Andrea, F., de Noblet-Ducoudré, N., 2012. Effects of interactive vegetation phenology on the 2003 summer heat waves. J. Geophys. Res. Atmos. 117 (D24).
Stephen, R., Anthony, B., 2002. Hierarchical Linear Models. Sage Publications, Thousand Oaks, CA.
Tran, D.X., Pla, F., Latorre-Carmona, P., Myint, S.W., Caetano, M., Kieu, H.V., 2017. Characterizing the relationship between land use land cover change and land surface temperature. ISPRS J Photogramm 124, 119–132.
Trlica, A., Hutyra, L.R., Schaaf, C.L., Erb, A., Wang, J.A., 2017. Albedo, land cover, and daytime surface temperature variation across an urbanized landscape. Earth's Future 5 (11), 1084–1101.
United States Geological Survey (Usgs), 2013. https://www.usgs.gov/land-resources/nli/landsat.
Valor, E., Caselles, V., 1996. Mapping land surface emissivity from NDVI: application to European, African, and South American areas. Remote Sens. Environ. 57, 167–184.
Weng, Q., 2009. Thermal infrared remote sensing for urban climate and environmental studies: methods, applications, and trends. ISPRS J Photogramm 64 (4), 335–344.
Wu, X., Guo, W., Liu, H., et al., 2019. Exposures to temperature beyond threshold disproportionately reduce vegetation growth in the northern hemisphere. Natl Sci Rev 6, 786–795.
Xu, H., Lin, D., Tang, F., 2013. The impact of impervious surface development on land surface temperature in a subtropical city: Xiamen, China. Int. J. Climatol. 33, 1873–1883.
Yang, Q., Huang, X., Tang, Q., 2018. The footprint of urban heat island effect in 302 Chinese cities: temporal trends and associated factors. Sci. Total Environ. 655, 652–662.
Yu, Z., Xu, S., Zhang, Y., Jorgensen, G., Vejre, H., 2018. Strong contributions of local background climate to the cooling effect of urban green vegetation. Sci. Rep. 8, 6798.
Yuan, F., Bauer, M.E., 2007. Comparison of impervious surface area and normalized difference vegetation index as indicators of surface urban heat island effects in Landsat imagery. Remote Sens. Environ. 106, 375–386.
Yue, W., Liu, X., Zhou, Y., Liu, Y., 2019. Impacts of urban configuration on urban heat island: an empirical study in China mega-cities. Sci. Total Environ. 671, 1036–1046.
Zhao, S., Liu, S., Zhou, D., 2016. Prevalent vegetation growth enhancement in urban environment. Proc. Natl. Acad. Sci. U. S. A. 113, 6313–6318.
Zhou, D., Zhao, S., Liu, S., Zhang, L., Zhu, C., 2014. Surface urban heat island in China's 32 major cities: spatial patterns and drivers. Remote Sens. Environ. 152, 51–61.
Zhou, D., Zhao, S., Zhang, L., Sun, G., Liu, Y., 2015. The footprint of urban heat island effect in China. Sci. Rep. 5, 11160.
Zhou, W., Wang, J., Cadenasso, M.L., 2017a. Effects of the spatial configuration of trees on urban heat mitigation: a comparative study. Remote Sens. Environ. 195, 1–12.
Zhou, B., Rybski, D., Kropp, J.P., 2017b. The role of city size and urban form in the surface urban heat island. Sci. Rep. 7, 4791.
Ziter, C.D., Pedersen, E.J., Kucharik, C.J., Turner, M.G., 2019. Scale-dependent interactions between tree canopy cover and impervious surfaces reduce daytime urban heat during summer. Proc. Natl. Acad. Sci. U. S. A. 116, 7575–7580.